

# Gallium-68-labeled Peptide PET Quantifies Tumor Exposure of PD-L1 Therapeutics



Akhilesh Mishra<sup>1,2</sup>, Dhiraj Kumar<sup>1</sup>, Kuldeep Gupta<sup>1</sup>, Gabriela Lofland<sup>1</sup>, Ajay Kumar Sharma<sup>1</sup>, Dhanush S. Banka<sup>1</sup>, Robert F. Hobbs<sup>3</sup>, Robert F. Dannals<sup>1</sup>, Steven P. Rowe<sup>1</sup>, Edward Gabrielson<sup>4,5</sup>, and Sridhar Nimmagadda<sup>1,5,6,7</sup>

## ABSTRACT

**Purpose:** Immune checkpoint therapy (ICT) is currently ineffective in a majority of patients. Tumor drug exposure measurements can provide vital insights into mechanisms involved in the resistance of solid tumors to those therapeutics; however, tools to quantify *in situ* drug exposure are few. We have investigated the potential of programmed death-ligand 1 (PD-L1) pharmacodynamics, quantified using PET, to inform on the tumor exposure of anti-PD-L1 (aPD-L1) therapeutics.

**Experimental Design:** To noninvasively quantify PD-L1 levels, we first developed a novel peptide-based gallium-68-labeled binder, [<sup>68</sup>Ga]Ga-DK223, and evaluated its *in vivo* distribution, pharmacokinetics, and PD-L1 specificity in preclinical models of triple-negative breast cancer and urothelial carcinoma with variable PD-L1 expression. We then quantified baseline and accessible PD-L1 levels in tumors as a noninvasive pharmaco-

dynamic measure to assess tumor exposure to two aPD-L1 antibodies (avelumab and durvalumab).

**Results:** DK223 exhibited a KD of 1.01±0.83 nmol/L for PD-L1 and inhibited the PD-1:PD-L1 interaction in a dose-dependent manner. [<sup>68</sup>Ga]Ga-DK223 provides high-contrast PET images within 60 minutes of administration and detects PD-L1 in an expression-dependent manner in xenograft models. PD-L1 pharmacodynamics measured using [<sup>68</sup>Ga]Ga-DK223-PET revealed that avelumab and durvalumab had similar exposure early during therapy, but only durvalumab exhibited sustained exposure at the tumor.

**Conclusions:** [<sup>68</sup>Ga]Ga-DK223 detected variable PD-L1 levels and exhibited salient features required for clinical translation. [<sup>68</sup>Ga]Ga-DK223-PET could be useful for quantifying total PD-L1 levels at baseline and accessible PD-L1 levels during therapy to understand drug exposure at the tumor, thus supporting its use for guiding and optimizing ICT.

## Introduction

The past two decades have seen an improved understanding of the roles of the host immune system in fighting cancer (1). mAbs targeting immune checkpoints have taken center stage in efforts to leverage that understanding for improving cancer therapy, and increasing numbers of agents are in development. Population pharmacokinetic studies are currently used to optimize the dosing regimens of those therapeutics (2). However, the exposure and activity of mAbs in tumors are poorly understood. Although pharmacokinetic data guide dosing

regimens, they provide virtually no information about drug exposure at the disease site. Given the poor penetration of mAbs within solid tumors and the heterogeneity of target expression within and across patients, *in situ* drug exposure measurements could enable personalized dosing and improved efficacy (3–5). Measures of drug exposure that are agnostic to the disease type and location, independent of the biophysical properties of mAbs, enable repeat sampling, and encompass all of the factors associated with heterogeneity of tumors may address an unmet clinical need (6, 7).

Immune checkpoint protein programmed death-ligand 1 (PD-L1, CD274) is one important target for therapeutic efforts in immunoncology, with three mAbs now regulatory approved (atezolizumab, avelumab, and durvalumab). PD-L1 expression is currently used as a biomarker to guide immune checkpoint therapy (ICT) in some cancers (8–11), but PD-L1 detection by IHC involves sampling a small fraction of the tumor and fails to capture total PD-L1 levels or heterogeneity in PD-L1 expression within and across patients (12, 13). Moreover, PD-L1 expression is dynamic and changes during the course of immunotherapy, suggesting that it could be beneficial to capture total PD-L1 levels and dynamics with use of noninvasive technologies, such as PET (14, 15). For example, clinical evaluation of [<sup>89</sup>Zr]atezolizumab showed that radiotracer uptake is heterogeneous within and across patients and that [<sup>89</sup>Zr]atezolizumab uptake in lesions is a better predictor of response to anti-PD-L1 (aPD-L1) therapy than genomics-derived biomarkers (16).

To complement these efforts, others and we have reported small protein- and peptide-based imaging agents that provide high-contrast images much sooner than mAb-derived radiotracers (17, 18). One such peptide-based radiotracer, [<sup>68</sup>Ga]WL12, showed PD-L1 dependent uptake in preclinical studies and in patients with non-small cell lung cancer (NSCLC) within 120 minutes of injection (19). In addition, our peptide-based radiotracers bind PD-L1 in a manner similar to that

<sup>1</sup>The Russell H. Morgan Department of Radiology and Radiological Science, Johns Hopkins University School of Medicine, Baltimore, Maryland. <sup>2</sup>Chemical & Biomolecular Engineering, Whiting School of Engineering, Johns Hopkins University, Baltimore, Maryland. <sup>3</sup>Radiation Oncology and Molecular Radiation Sciences, Johns Hopkins University School of Medicine, Baltimore, Maryland. <sup>4</sup>Department of Pathology, Johns Hopkins University School of Medicine, Baltimore, Maryland. <sup>5</sup>The Sidney Kimmel Comprehensive Cancer Center and the Bloomberg-Kimmel Institute for Cancer Immunotherapy, Johns Hopkins University School of Medicine, Baltimore, Maryland. <sup>6</sup>Department of Pharmacology and Molecular Sciences, Johns Hopkins University School of Medicine, Baltimore, Maryland. <sup>7</sup>Division of Clinical Pharmacology, Department of Medicine, Johns Hopkins University School of Medicine, Baltimore, Maryland.

A. Mishra and D. Kumar contributed equally as co-first authors of this article.

**Corresponding Author:** Sridhar Nimmagadda, Johns Hopkins Medical Institutions, 1550 Orleans Street, CRB II, #492, Baltimore, MD 21287. Phone: 410-502-6244, Fax: 410-614-3147, E-mail: snimmag1@jhmi.edu

Clin Cancer Res 2023;29:581-91

doi: 10.1158/1078-0432.CCR-22-1931

This open access article is distributed under the Creative Commons Attribution-NonCommercial-NoDerivatives 4.0 International (CC BY-NC-ND 4.0) license.

©2022 The Authors; Published by the American Association for Cancer Research

### Translational Relevance

mAbs against immune checkpoint proteins have transformed cancer treatment, but only a subset of patients with cancer benefit from such immunotherapy. Although much research has focused on the genetic and molecular basis of resistance to immune checkpoint therapeutics, failure to achieve sufficient drug exposure at the tumor site also contributes to acquired resistance. *In situ* drug exposure is difficult to measure, and recognizing the need for real-time quantitation of drug exposure at the tumor, we developed a gallium-68-labeled peptide radiotracer, [<sup>68</sup>Ga]Ga-DK223, which provides high-contrast images of programmed death-ligand 1 (PD-L1) expression by PET. Using [<sup>68</sup>Ga]Ga-DK223 PET, we demonstrated that the pharmacodynamics of PD-L1 can be used to noninvasively evaluate the exposure of anti-PD-L1 mAbs at the tumor. Our pharmacodynamics-based approach has broader implications for patient selection, guiding therapy, and accelerating the development of new checkpoint inhibitor mAbs.

of endogenous receptor programmed death protein 1 (PD-1) and aPD-L1 therapeutics (20). This unique binding mode enabled us to quantify the target engagement of aPD-L1 therapeutics by measuring accessible PD-L1 levels (target levels not occupied by mAbs) using PET. All three approved PD-L1 mAbs fit a two-compartment linear clearance pharmacokinetic model, but their temporal kinetics in the tumor remain to be characterized (21).

Here, we report the development of a new gallium-68-labeled peptide-based radiotracer for PD-L1 that shows substantially improved pharmacokinetic properties compared with previously reported agents. We evaluated the pharmacokinetics, biodistribution, and PD-L1 specificity of [<sup>68</sup>Ga]Ga-DK223 *in vitro* and *in vivo* using multiple cell lines and xenografts with variable PD-L1 levels derived from triple-negative breast cancer (TNBC) and urothelial carcinoma (UC). Moreover, we evaluated whether accessible PD-L1 levels within the tumor microenvironment, measured using [<sup>68</sup>Ga]Ga-DK223 PET, inform the temporal kinetics of drug exposure of two PD-L1 mAbs (avelumab and durvalumab) in the tumor, where it is most relevant (1).

## Materials and Methods

### Chemicals

DK221 [Cyclo(-Ac-Tyr-NMeAla-Asn-Pro-His-Glu-Hyp-Trp-Ser-Trp(Carboxymethyl)-NMeNle-NMeNle-Lys)-Gly-NH<sub>2</sub>] was custom synthesized by CPC Scientific (Sunnyvale, CA) with > 95% purity. 1,4,7,10-Tetraazacyclododecane-1,4,7,10-tetraacetic acid mono-N-hydroxysuccinimide ester (DOTA-NHS ester) and 2,2',2''-(10-(2,6-dioxotetrahydro-2H-pyran-3-yl)-1,4,7,10-tetraazacyclododecane-1,4,7-triyl)triacetic acid (DOTA-GA anhydride) were purchased from Macrocyclics (# B-280) and CheMatech (#C109), respectively. All other chemicals were purchased from Sigma-Aldrich or Fisher Scientific.

### Synthesis of DK223

In a reaction vial, to a stirred solution of DK221 (5.0 mg, 2.55 μmol) in dimethylformamide (1.0 mL), was added diisopropylethylamine (0.66 mg, 5.1 μmol) followed by DOTA-NHS Ester (3.0 mg, 3.8 μmol). The reaction mixture was stirred for 2 hours at room temperature. The reaction mixture was concentrated using a Rotavapor before purification on a reverse-phase high-performance liquid chromatography

(RP-HPLC) system using a semi-preparative C-18 Luna column (5 mm, 10 × 250 mm Phenomenex, Torrance, CA). The HPLC method used gradient elution starting with 20% acetonitrile (0.1% TFA) and reaching 60% in 25 minutes at a flow rate of 5 mL/min co-buffered with water (0.1% TFA). The desired DK223 was collected at 8.3 minutes, solvent evaporated under reduced pressure, residue reconstituted in 20% acetonitrile, and lyophilized to powder form with 68% yield. Purified DK223 was characterized by matrix-assisted laser desorption/ionization time-of-flight mass spectrometry (MALDI-TOF MS). Calculated [M+H]<sup>+</sup>:2343.61; observed:2343.62.

### Synthesis of DK397

In a reaction vial, to a stirred solution of DK223 (1.0 mg, 0.42 μmol) in 1M NaOAc buffer pH 4.0 was added 10 μL of 0.1 mol/L GaCl<sub>3</sub> solution. The reaction mixture was then heated at 95°C for 10 minutes. After cooling reaction mixture was loaded onto activated C18 Sep-pack, washed with 5 mL de-ionized water, and eluted with 90% acetonitrile. The solvent was evaporated under reduced pressure, residue reconstituted in 20% acetonitrile and lyophilized to form an off-white powder with 90% yield. The final product was characterized using MALDI-TOF. Calculated [M+H]<sup>+</sup>:2410.31; observed:2410.95. The DK397 complex was then used to optimize RP-HPLC conditions as a standard for radiolabeling and for PD-L1 and PD-1 competition binding assays.

### Synthesis of [<sup>68</sup>Ga]Ga-DK223 and [<sup>68</sup>Ga]Ga-DK385

The <sup>68</sup>Ge/<sup>68</sup>Ga generator was eluted manually using 6 mL of 0.1 mol/L HCl (ultrapure trace-metal-free) by fractional elution (1 mL/fraction). To a reaction vial (5 mL) containing 200 μL of 1 mol/L sodium acetate buffer (NaOAc; pH 5.5) and 20 to 40 μg of DK223, 7–19 mCi <sup>68</sup>GaCl<sub>3</sub> was added (1 mL fraction eluate). Ascorbic acid (50 μg) was added as a stabilizer to quench free radicals. The reaction mixture was then incubated for 10 minutes at 100°C in a temperature-controlled heating block. The reaction vial was cooled initially at room temperature for 1 minute followed by 2 to 3 minutes in cold water and quenched with 20% acetonitrile in water. The crude reaction mixture was purified on an RP-HPLC system using a semi-preparative C-18 Luna column (5 mm, 10 × 250 mm Phenomenex, Torrance, CA). The HPLC gradient elution started with 25% acetonitrile (0.1% formic acid) and reached 60% in 15 minutes at a flow rate of 5 mL/min, co-buffered with water (0.1% formic acid). The radiolabeled product was collected at 6.63 minutes, evaporated under stream of N<sub>2</sub> at 60°C and formulated in 5% EtOH in saline. [<sup>68</sup>Ga]Ga-DK223 was obtained with a non-decay radiochemical yield of 20%±5% (n = 37) and > 95% radiochemical purity. The formulated tracer was used for both *in vitro* and *in vivo* studies. [<sup>68</sup>Ga]Ga-DK385 was similarly synthesized using fractional elution method with a non-decay radiochemical yield of 26%±7% (n = 7) and > 95% radiochemical purity. For stability studies, see Supplementary Methods.

### Surface plasmon resonance analysis

Surface plasmon resonance (SPR) analysis was carried out using the Biacore Molecular Interaction Shared Resource at Georgetown University. All experiments were performed using a Biacore T200 instrument equipped with a CM5 chip at 25°C. Human PD-L1 Fc-tagged (52 kDa, 1.93 μmol/L stock concentration) was used as a ligand for capture onto the CM5 chip. DK223 (2,342.6 Da, 10 mmol/L stock concentration), DK385 (2,414.7 Da, 10 mmol/L stock concentration), and DK397 (2,409.31 Da, 10 mmol/L stock concentration) were used as analytes to flow over the ligand-capture surface. Flow cell (FC) 1 was used as the reference for FC2. Protein A/G was diluted (1:25 dilution,

1  $\mu\text{mol/L}$  diluted concentration) in 10 mmol/L sodium acetate buffer at pH 4.5, and immobilized on FC1 and FC2 to a level of  $\sim 4,400$  RU using standard amine coupling chemistry. PBS-P (20 mmol/L phosphate buffer pH 7.4, 137 mmol/L NaCl, 2.7 mmol/L KCl, 0.05% v/v surfactant P20) was used as the immobilization running buffer. Human PD-L1 was diluted (1:10 dilution) in PBS-P captured on FC2 to  $\sim 1,200$  RU. PBS-P was used as the capture buffer. On the basis of these captured response values, theoretical  $R_{\text{max}}$  values were calculated assuming a 1:1 interaction mechanism. The flow rate of all the analyte solutions was maintained at 50  $\mu\text{L}/\text{min}$ . The contact and dissociation times used were 120 seconds and 360 seconds, respectively. Glycine pH 2.0 was injected for 15 seconds for surface regeneration. This regeneration condition removes all the captured ligands from FC2. Therefore, fresh ligands are captured at the beginning of each injection cycle. The injected analyte concentrations ranged from 20 nmol/L to 0.625 nmol/L (two-fold dilutions). All analytes were injected in duplicates. For analysis, sensorgrams from the overnight kinetics were evaluated using 1:1 kinetics model fitting.

#### PD-L1 and PD-1 binding inhibition assay

A competitive inhibition assay for PD-L1 binding to PD-1 was optimized from a previously described fluorescence resonance energy transfer (FRET)-based assay in discussion with Cisbio (22) using PD-1-Ig and PD-L1-His-tag that were detected by anti-human IgG-Eu<sup>3+</sup> cryptate and anti-6HIS-XL665 monoclonal antibodies using a Perkin Elmer Victor3 1420 multi-label counter (PerkinElmer, Waltham, MA).

#### Cell culture reagents and antibodies

All cell culture reagents were purchased from Invitrogen (Carlsbad, CA). The aPD-L1 mAbs avelumab and durvalumab were purchased from the Johns Hopkins School of Medicine Pharmacy.

#### Cell culture

All cell lines were purchased from ATCC and cultured in the recommended medium in an incubator at 37°C in an atmosphere containing 5% CO<sub>2</sub>. MDAMB231, SCaBER, and BFTC909 cells were maintained in DMEM. SUM149 was a gift from Dr. Stephen Ethier and maintained in Ham's F-12K medium. A549, A549<sup>IPD-L1</sup>, CHO, and CHO<sup>hPD-L1</sup> were cultured as described previously (20). All cells were supplemented with 10% FBS and 1% P/S antibiotic. All cell lines were routinely tested for *Mycoplasma*. Freshly thawed cells were cultured for less than 3 months or authenticated at JHU Genomics Core.

#### Detection of PD-L1 expression by flow cytometry

Adherent cells were detached using enzyme-free cell dissociation buffer (Thermo Fisher Scientific, Waltham, MA). PD-L1 surface expression was evaluated by direct staining of  $1 \times 10^6$  cells in 100  $\mu\text{L}$  FACS buffer (PBS with 0.1% FBS and 2 mmol/L ethylenediaminetetraacetic acid) with aPD-L1 antibody (clone: MIH1 BD # 558065) for 30 minutes at 4°C. The cells were then washed and analyzed for mean fluorescence intensity by flow cytometry.

#### In vitro binding assays with [<sup>68</sup>Ga]Ga-DK223

*In vitro* binding of [<sup>68</sup>Ga]Ga-DK223 to MDAMB231, BFTC909, SUM149, and SCaBER cells was determined by incubating  $1 \times 10^6$  cells with approximately 1  $\mu\text{Ci}$  [<sup>68</sup>Ga]Ga-DK223 for 45 minutes at 4°C. After incubation, cells were washed 3 times with ice-cold PBS containing 0.1% tween 20 and counted on an automated gamma counter. Percentage of incubated activity (%IA) was calculated on the basis of signal decay correction and normalization to external [<sup>68</sup>Ga]Ga-

DK223 standards measured in quadruplicate. All cell radioactivity uptake studies were performed in quadruplicate for each cell line and repeated 3 times.

#### Receptor density measurements

Phycoerythrin Fluorescence Quantitation Kit (BD Biosciences, #340495) containing four levels of phycoerythrin/bead were used. Beads were reconstituted, with 0.5 mL of PBS containing sodium azide and 0.5% bovine serum albumin, just before use. Cells were stained for 30 minutes at 4°C with phycoerythrin-labeled aPD-L1 antibody (clone: MIH1 BD # 558065) and run along with the beads to estimate receptor density using flow cytometry. Calibration curve of geometric mean versus phycoerythrin/bead from different bead populations was generated as per the manufacturer's protocol. This calibration curve was used to derive receptors/cell for each cell type from their respective geometric means. Isotype controls were used to eliminate any non-specific staining. PD-L1 receptor density measured above was then correlated with [<sup>68</sup>Ga]Ga-DK223 %IA uptake measured in *in vitro* binding assays.

#### In vivo studies

All mouse studies were conducted using protocols approved by the Johns Hopkins University Animal Care and Use Committee. Xenografts were established in 5- to 6-week-old, male (UC) or female (TNBC), NSG mice obtained from Johns Hopkins University Immune Compromised Animal Core.

#### Xenograft models

Mice were subcutaneously injected with cancer cells in 100  $\mu\text{L}$  saline (top right flank, unless otherwise noted) in all tumor models. The following cell lines were used: A549 ( $5 \times 10^6$ ), A549<sup>IPD-L1</sup> ( $5 \times 10^6$ ), CHO ( $10 \times 10^6$ ), CHO<sup>hPD-L1</sup> ( $10 \times 10^6$ ), MDAMB231 ( $1 \times 10^6$ ), SUM149 ( $2 \times 10^6$ ), BFTC909 ( $1 \times 10^6$ ), and SCaBER ( $5 \times 10^6$ ). Mice with tumor volumes of 100 to 200 mm<sup>3</sup> were used for treatment, PET imaging, and *ex vivo* biodistribution experiments.

#### PET-CT imaging of mouse xenografts

Mice with 100 to 200 mm<sup>3</sup> tumor volume were injected with 200  $\mu\text{Ci}$  (7.4 MBq) of [<sup>68</sup>Ga]Ga-DK223 in 200  $\mu\text{L}$  of 5% ethanol in saline intravenously and anesthetized with 2.5% isoflurane. PET images were acquired 60 minutes after radiotracer injection for 10 minutes in one or two bed positions (whole body) using an ARGUS small-animal PET/CT scanner (Sedecal, Madrid, Spain). PET data were reconstructed using the two-dimensional ordered subset expectation maximization algorithm and corrected for radioactive decay and dead time. The percentage of incubated dose per cubic centimeter (%ID/cc) values were calculated on the basis of the calibration factor obtained from a known radioactive quantity. Image fusion, visualization, and 3D rendering were accomplished using Amira 6.1 (FEI, Hillsboro, OR).

#### Ex vivo biodistribution

To validate the imaging studies, *ex vivo* biodistribution studies were conducted in mice with at least 100 to 200 mm<sup>3</sup>. The mice received 80  $\mu\text{Ci}$  (2.96 MBq) [<sup>68</sup>Ga]Ga-DK223 for dosimetry studies and 50  $\mu\text{Ci}$  (1.85 MBq) for all other biodistribution studies. Total mass of non-radioactive peptide varied from 0.03 to 0.15  $\mu\text{g}/\text{kg}$ . All injections were in 200  $\mu\text{L}$  of 5% ethanol in saline intravenously, and biodistribution studies were conducted at specified time points for radiotracer pharmacokinetic studies and at 60 minutes after [<sup>68</sup>Ga]Ga-DK223 injection for all other studies ( $n = 4-5$ ). Selected tissues (the heart, lung, liver,

stomach, spleen, pancreas, kidney, small intestine, testicles, and muscle), tumors, and blood were collected, weighed, and counted, and their incubated dose per gram (%ID/g) values were calculated on the basis of signal decay correction and normalization to external [ $^{68}\text{Ga}$ ]Ga standards measured in triplicate.

### IHC

Tumor sections were evaluated for PD-L1 expression by IHC as reported previously (11). Briefly, 4–5- $\mu\text{m}$  tumor sections were treated with 3%  $\text{H}_2\text{O}_2$  for 10 minutes, blocked with 5% goat serum for 1 hour, and then incubated with a primary anti-human PD-L1 antibody (#13684, Cell Signaling Technology) at 1:500 dilution at 4°C overnight. Subsequently, using Dako CSAII Biotin-free Tyramide Signal Amplification System Kit, slides were incubated with secondary antibody and amplification reagent. Final staining was carried out by adding 3,3'-Diaminobenzidine.

### *In vivo* stability of [ $^{68}\text{Ga}$ ]Ga-DK223

[ $^{68}\text{Ga}$ ]Ga-DK223 ( $R_t = 7.43$  minutes) was generated with more than 99% radiochemical purity. Stability studies were conducted by injecting  $250 \pm 17 \mu\text{Ci}$  of [ $^{68}\text{Ga}$ ]Ga-DK223 intravenously ( $n = 3$ ). At 60 minutes, 6  $\mu\text{L}$  of urine was collected having  $24 \pm 8 \mu\text{Ci}$  of activity which was diluted 3x with cold ethanol followed by syringe filtration. The filtered urine sample further diluted 10x with water and injected into HPLC. The radio HPLC chromatogram of urine sample showed intact tracer ( $R_t = 7.34$  minutes) and no radioactive side peaks.

### Effect of nonradioactive DK223 on [ $^{68}\text{Ga}$ ]Ga-DK223 uptake in tumors

[ $^{68}\text{Ga}$ ]Ga-DK223 was coadministered with nonradioactive DK223 at doses of 0, 1.2, 4, 12, and 1,200  $\mu\text{g}/\text{kg}$ , and uptake was assessed in BFTC909 UC xenografts using PET imaging.

### iPD-L1 imaging treatment in A549 xenografts

NSG male mice harboring subcutaneous A549 and A549<sup>hPD-L1</sup> tumors were treated daily with 200  $\mu\text{L}$  of 10 mg/mL doxycycline solution by oral gavage ( $n = 3/\text{group}$ ). PET-CT imaging was performed 48 hours after treatment.

### aPD-L1 treatment in BFTC909 xenografts

NSG male mice harboring subcutaneous BFTC909 tumors were treated with a 10 mg/kg dose of avelumab, durvalumab, or saline

injected intravenously ( $n = 6/\text{group}$ ). PET-CT imaging was performed every day after treatment for up to 5 days. For biodistribution studies, mice were treated on days 1, 2, 3, 4, and 5 and sacrificed on day 6, resulting in 120, 96, 72, 48, and 24 hours of treatment, respectively.

### Statistical analysis

All statistical analyses were performed using Prism 8 (GraphPad Software, La Jolla, CA). Unpaired Student *t* test and one- or two-way ANOVA were used for column, multiple column, and grouped analyses, respectively. Statistical significance was set at  $P < 0.05$ . Correlation was performed using simple linear regression without keeping the term constant at zero.

### Data availability

All study data are included in the article and/or supplementary information. Additional data are available upon request from the corresponding author.

## Results

### Synthesis and characterization of DK223 as PD-L1 binding moiety

DK223 is derived from DK221, a 14 amino acid cyclic peptide with a free lysine amine, that has demonstrated specificity for human PD-L1 (23, 24). To evaluate the effect of chelators on binding affinity and *in vivo* pharmacokinetics, the free lysine amine of DK221 was conjugated to DOTA or DOTAGA chelators to effectively bind gallium-68 to produce [ $^{68}\text{Ga}$ ]Ga-DK223 or [ $^{68}\text{Ga}$ ]Ga-DK385, respectively, as well as the nonradioactive analog DK397 (Fig. 1A; Supplementary Fig. S1A–S1L). DK223 and DK385 bound to PD-L1 with a dissociation constant of  $1.01 \pm 0.83$  nmol/L and  $5.7 \pm 0.91$  nmol/L, respectively, as per SPR analysis (Fig. 1B). DK223 and DK385 also inhibited the PD-1:PD-L1 interaction in a dose-dependent manner, with an  $\text{IC}_{50}$  of  $27 \pm 4.9$  nmol/L (Fig. 1C). The radiolabeled products [ $^{68}\text{Ga}$ ]Ga-DK223 and [ $^{68}\text{Ga}$ ]Ga-DK385 were obtained with non-decay corrected radiochemical yields of  $20\% \pm 5\%$  ( $n = 37$ ) and  $26\% \pm 7\%$  ( $n = 7$ ), respectively, with  $>95\%$  radiochemical purity. We observed a moderate specific activity (molar activity) of 10.36 GBq/ $\mu\text{mol}$  (280 mCi/ $\mu\text{mol}$ ) with [ $^{68}\text{Ga}$ ]Ga-DK223. The formulated [ $^{68}\text{Ga}$ ]Ga-DK223 dose was stable for 4 hours (Supplementary Fig. S1M).

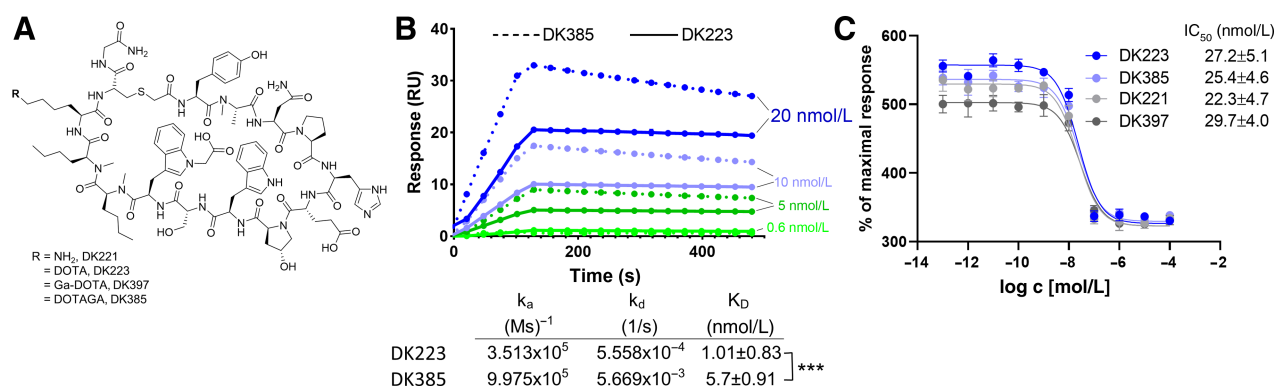
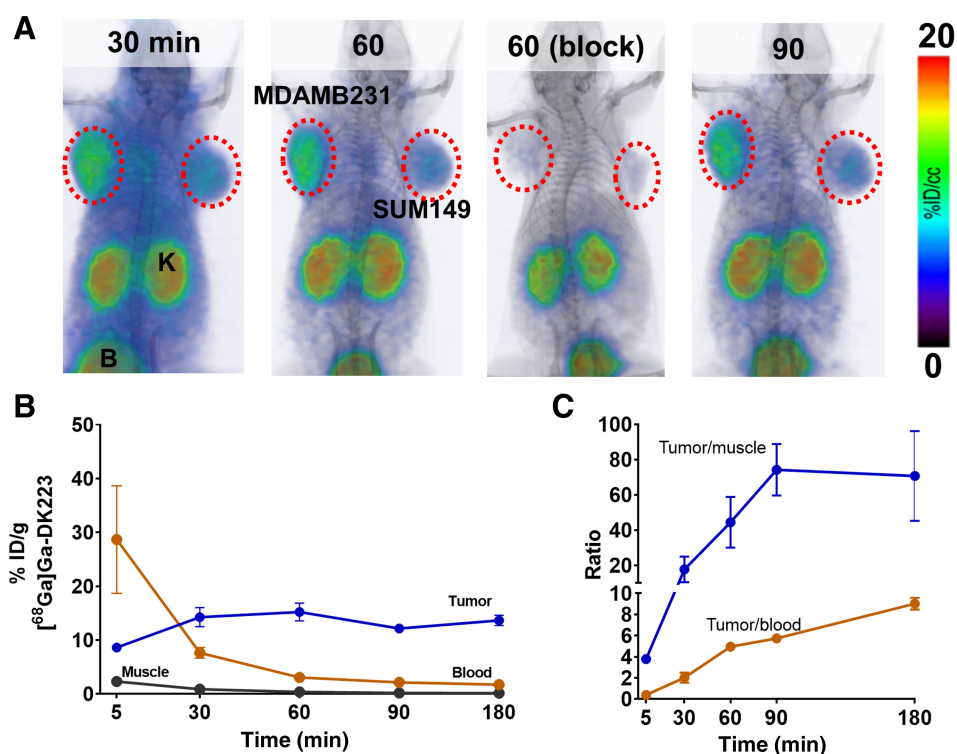


**Figure 1.**

Synthesis and *in vitro* characterization of DK221 derivatives. **A**, Structures of parent peptide DK221 and its analogs. **B**, SPR analysis of DK223 ( $n = 3$ ) and DK385 ( $n = 3$ ) binding to PD-L1. **C**, Fluorescence resonance energy transfer (FRET)-based assay showing sub-nanomolar affinities for DK221 ( $n = 3$ ), DK223 ( $n = 3$ ), DK385 ( $n = 3$ ), and DK397 ( $n = 3$ ) for inhibiting PD-1:PD-L1 interaction. \*\*\*,  $P < 0.001$  by Student *t* test.

**Figure 2.**

Pharmacokinetics of [ $^{68}\text{Ga}$ ]Ga-DK223. **A**, PET-CT images in NSG mice bearing MDAMB231 (left flank) and SUM149 (right flank) tumors at different time points show high tumor-to-background ratio at 60 minutes after injecting [ $^{68}\text{Ga}$ ]Ga-DK223. Radioactivity uptake reduced in MDAMB231 tumors after blocking with unlabeled 50  $\mu\text{g}$  DK223 confirming PD-L1 specificity. Mice were injected with  $\sim 7.4$  MBq ( $\sim 200$   $\mu\text{Ci}$ ) [ $^{68}\text{Ga}$ ]Ga-DK223 (B, bladder; K, kidney;  $n = 3$ ). **B**, Pharmacokinetics of [ $^{68}\text{Ga}$ ]Ga-DK223 in tumor, blood, and muscle, and **C**, tumor-to-tissue ratios. For **B** and **C**, mice were injected with  $\sim 740$  kBq ( $\sim 50$   $\mu\text{Ci}$ ) [ $^{68}\text{Ga}$ ]Ga-DK223 and sacrificed at different time points after injection ( $n = 4$ –5).



### Pharmacokinetics of [ $^{68}\text{Ga}$ ]Ga-DK223

Biodistribution studies conducted with [ $^{68}\text{Ga}$ ]Ga-DK385 showed less tumor uptake ( $8.50 \pm 1.67\%$  ID/g) and tumor-to-muscle ( $19.86 \pm 2.15$ ) and tumor-to-blood ( $2.32 \pm 0.38$ ) ratios at 60 minutes compared with [ $^{68}\text{Ga}$ ]Ga-DK223 (Supplementary Fig. S2A). Thus, we pursued detailed evaluation of [ $^{68}\text{Ga}$ ]Ga-DK223.

[ $^{68}\text{Ga}$ ]Ga-DK223 is specific to hPD-L1 and lacks reactivity towards mPD-L1 (Supplementary Fig. S2B–S2D). Therefore, to evaluate the pharmacokinetics, biodistribution, and *in vivo* specificity of [ $^{68}\text{Ga}$ ]Ga-DK223 for binding PD-L1, we used immunodeficient NSG mice with MDAMB231 human TNBC xenografts expressing PD-L1 (Fig. 2A). PET images of MDAMB231 tumor-bearing mice injected with [ $^{68}\text{Ga}$ ]Ga-DK223 revealed high radiotracer accumulation in tumors as early as 5 minutes after injection. A higher tumor contrast was observed at 60 minutes owing to background radiotracer clearance. Administration of 2 mg/kg nonradioactive DK223 reduced tracer uptake in MDAMB231 xenografts demonstrating the specificity of [ $^{68}\text{Ga}$ ]Ga-DK223 for PD-L1. In comparison, low PD-L1-expressing SUM149 tumors showed low levels of uptake, similar to levels seen in non-PD-L1-expressing tissues such as muscle. Kidney and bladder tissues showed the highest radiotracer accumulation among normal tissues, consistent with the renal clearance mechanism for low-molecular-weight peptides. To confirm the PET results, *ex vivo* biodistribution studies were performed (Table 1). [ $^{68}\text{Ga}$ ]Ga-DK223 uptake reached a maximum of  $15.21 \pm 1.43\%$  ID/g in MDAMB231 tumors at 60 minutes and demonstrated high tumor retention even at 180 minutes (Fig. 2B). Blood pool activity showed consistent washout, with nearly 90% of activity cleared by 60 minutes. Similar radioactivity washouts were observed in all other nonspecific tissues. Consequently, the tumor-to-blood and tumor-to-muscle ratios were the highest between 60 and 180 minutes (Fig. 2C). The *in vivo* stability of [ $^{68}\text{Ga}$ ]Ga-DK223 was also measured in urine collected at 60 minutes, which showed

no metabolic cleavage (Supplementary Fig. S2E). Therefore, we used the 60-minute time point for all further experiments, as it provided good contrast and fits within the standard PET clinical workflow.

### Human radiation dosimetry estimates

Pharmacokinetic data evaluated from MDAMB231 tumor-bearing mice were decay-corrected and used to calculate the residence times of [ $^{68}\text{Ga}$ ]Ga-DK223 in human organs (Table 1; Supplementary Fig. S2F). We then used these residence times as inputs for OLINDA/EXM software to obtain absorbed organ doses for gallium-68 in the adult reference human female phantom. The predicted absorbed doses in the human organs are listed in Table 1 and Supplementary Fig. S2G. The organs receiving the maximum dose were the kidneys (0.21 rem/mCi), followed by the lungs (0.07 rem/mCi), heart wall (0.06 rem/mCi), and thymus (0.04 rem/mCi). On the basis of these findings, a 20 mCi dose can be administered with an effective dose equivalent estimate of less than 5 rem to acquire PET images in human subjects.

### Evaluation of [ $^{68}\text{Ga}$ ]Ga-DK223 in UC and TNBC cancer xenografts

Next, we validated the ability of [ $^{68}\text{Ga}$ ]Ga-DK223 to detect variable levels of PD-L1 *in vivo*, using xenografts of two TNBC cell lines (MDAMB231 and SUM149) and two UC cell lines (BFTC909 and SCaBER). PD-L1 levels in these cell lines measured using flow cytometry (Fig. 3A; Supplementary Fig. S3A) were in the following order: BFTC909 > MDAMB231 > SCaBER > SUM149. Cells incubated with [ $^{68}\text{Ga}$ ]Ga-DK223 showed highest levels of uptake in BFTC909 ( $28.9 \pm 0.55\%$  IA), followed by MDAMB231 ( $21.4 \pm 0.57$ ), and less than 2% IA in SCaBER and SUM149 cells, in agreement with flow cytometry data (Fig. 3B). Cells incubated with 1  $\mu\text{mol/L}$  nonradioactive DK223 showed significantly reduced [ $^{68}\text{Ga}$ ]Ga-DK223 uptake ( $P < 0.0001$ ), confirming the uptake specificity of the radiotracer. To establish relevance of PD-L1 expression to radioactivity uptake, we measured

**Table 1.** Pharmacokinetics of [<sup>68</sup>Ga]Ga-DK223 in mice with MDAMB231 xenografts and predicted residence times in human organs with respective absorbed doses.

Tissues	%ID/g [ <sup>68</sup> Ga]Ga-DK223 time (minutes)						Residence time (h)	Organ dose (rem/mCi)
	5	30	60	60 (block)	90	180		
Blood	28.67 ± 8.65	7.63 ± 0.87	3.05 ± 0.11	1.09 ± 0.18	2.14 ± 0.08	1.72 ± 0.04	0.17533	n/a
Muscle	2.29 ± 0.09	0.85 ± 0.09	0.36 ± 0.04	0.85 ± 0.07	0.17 ± 0.01	0.08 ± 0.02	0.06168	0.0083
Tumor	8.62 ± 0.29	14.26 ± 1.54	15.21 ± 1.43	0.04 ± 0.01	12.15 ± 0.32	11.59 ± 0.79	n/a	n/a
Lung	14.83 ± 0.4	11.03 ± 2.29	4.7 ± 0.42	0.57 ± 0.1	5.3 ± 1.68	2.98 ± 0.71	0.03245	0.0705
Thymus	9.96 ± 0.82	7.02 ± 1.06	3.53 ± 0.27	2.76 ± 0.16	1.26 ± 0.47	1.52 ± 0.75	0.00047	0.0434
Heart	6.39 ± 0.35	2.49 ± 0.3	0.95 ± 0.07	2.42 ± 0.4	0.73 ± 0.03	0.46 ± 0.03	0.0151	0.0558
Liver	5.63 ± 0.29	2.85 ± 0.41	1.31 ± 0.08	0.99 ± 0.14	0.91 ± 0.11	0.82 ± 0.09	0.01633	0.0252
Stomach (with contents)	2.2 ± 0.16	1.39 ± 0.31	0.65 ± 0.09	0.35 ± 0.07	0.46 ± 0.09	0.37 ± 0.04	0.00072	0.0061
Pancreas	3.04 ± 0.11	2.01 ± 0.54	0.45 ± 0.05	0.41 ± 0.02	0.39 ± 0.01	0.24 ± 0.03	0.00052	0.015
Spleen	3.69 ± 0.13	2.45 ± 0.51	1.05 ± 0.07	0.91 ± 0.07	0.71 ± 0.06	0.58 ± 0.03	0.00129	0.0196
Small intestine (with contents)	3.41 ± 0.37	1.64 ± 0.32	0.65 ± 0.2	0.44 ± 0.04	0.96 ± 0.09	0.74 ± 0.17	0.00453	0.013
Large intestine (with contents)	2.01 ± 0.16	0.79 ± 0.1	0.52 ± 0.09	0.29 ± 0.06	0.42 ± 0.1	1.74 ± 0.37	0.00099	0.0084
Adrenals	4.18 ± 0.26	2.22 ± 0.19	4.74 ± 3.64	1.32 ± 0.09	0.18 ± 0.03	0.16 ± 0.11	0.00014	0.0181
Kidney	28.59 ± 2.4	24.4 ± 1.5	22.99 ± 2.01	26.34 ± 0.19	16.23 ± 0.8	19.14 ± 1.32	0.0337	0.21
Ovaries	6.1 ± 0.55	2.69 ± 0.34	0.93 ± 0.08	2.92 ± 0.79	0.47 ± 0.09	0.27 ± 0.18	0.00011	0.017
Uterus	7.48 ± 1.37	3.82 ± 0.57	1.52 ± 0.26	1.03 ± 0.06	1.13 ± 0.09	0.47 ± 0.03	0.00114	0.0253
Bladder	5.74 ± 0.71	4.09 ± 0.49	1.42 ± 0.12	2.69 ± 1.82	0.78 ± 0.07	1.28 ± 0.32	0.00187	0.0081
Femur	10.58 ± 5.79	1.74 ± 0.14	0.89 ± 0.06	0.34 ± 0.03	0.59 ± 0.04	0.64 ± 0.07	0.03956	0.0333
Brain	0.65 ± 0.08	0.22 ± 0.05	0.08 ± 0.01	0.44 ± 0.09	0.05 ± 0.01	0.04 ± 0.01	0.00118	0.0029

Note: *Ex vivo* biodistribution studies in NSG mice bearing MDAMB231 tumors. Mice were injected with ~740 kBq (~50 μCi) [<sup>68</sup>Ga]Ga-DK223 and sacrificed after corresponding time point ( $n = 4-5$ ). Blocking was performed by treating mice with nonradioactive 50 μg DK223. Residence time and equivalent human organ dose was calculated using OLINDA/XEM software.

cell surface PD-L1 density (Fig. 3C) and found a strong correlation between PD-L1 density and [<sup>68</sup>Ga]Ga-DK223 uptake ( $R^2 = 0.9370$ ). Taken together, these cell-based assays provide evidence for the potential of [<sup>68</sup>Ga]Ga-DK223 to detect variable PD-L1 levels.

To validate those *in vitro* results, we performed PET imaging of tumor xenografts derived from the same four cell lines (Fig. 3D). We observed the highest uptake of [<sup>68</sup>Ga]Ga-DK223 in BFTC909 tumors, followed by MDAMB231, which was also confirmed by region of interest analyses of the tumors (Supplementary Fig. S3B and S3C). Tumors of low PD-L1-expressing SCaBER and SUM149 cell lines showed correspondingly low radiotracer uptake. IHC staining of the same xenografts for PD-L1 corroborated the PET data (Fig. 3E). Next, *ex vivo* biodistribution studies were performed to validate the imaging findings. We found that the tumor uptake was in agreement with the *in vitro* and PET results, with the highest uptake observed with BFTC909 ( $21 \pm 2.1\%$ ID/g), followed by MDAMB231 ( $11 \pm 1.6\%$ ID/g). In contrast, SCaBER and SUM149 tumors showed less than  $3\%$ ID/g of [<sup>68</sup>Ga]Ga-DK223, consistent with their low PD-L1 status. Tumor-to-muscle and tumor-to-blood ratios showed similar trends with respect to PD-L1 status (Fig. 3F), and background tissues showed no significant differences between tumor models (Supplementary Fig. S3D and S3E). Further analysis showed an absence of a positive correlation between tumor mass and %ID/g, indicating that uptake of [<sup>68</sup>Ga]Ga-DK223 in BFTC909 and MDAMB231 xenografts was not size-dependent but rather PD-L1 specific (Supplementary Fig. S3F and S3G). We also evaluated the effect of precursor mass (i.e., effective specific activity) on the uptake of [<sup>68</sup>Ga]Ga-DK223 in BFTC909 xenografts. We observed that 12 μg/kg of nonradioactive DK223, a human equivalent dose of 1.15 μg/kg, had a minimal effect on [<sup>68</sup>Ga]Ga-DK223 uptake in tumors (Supplementary Fig. S3H).

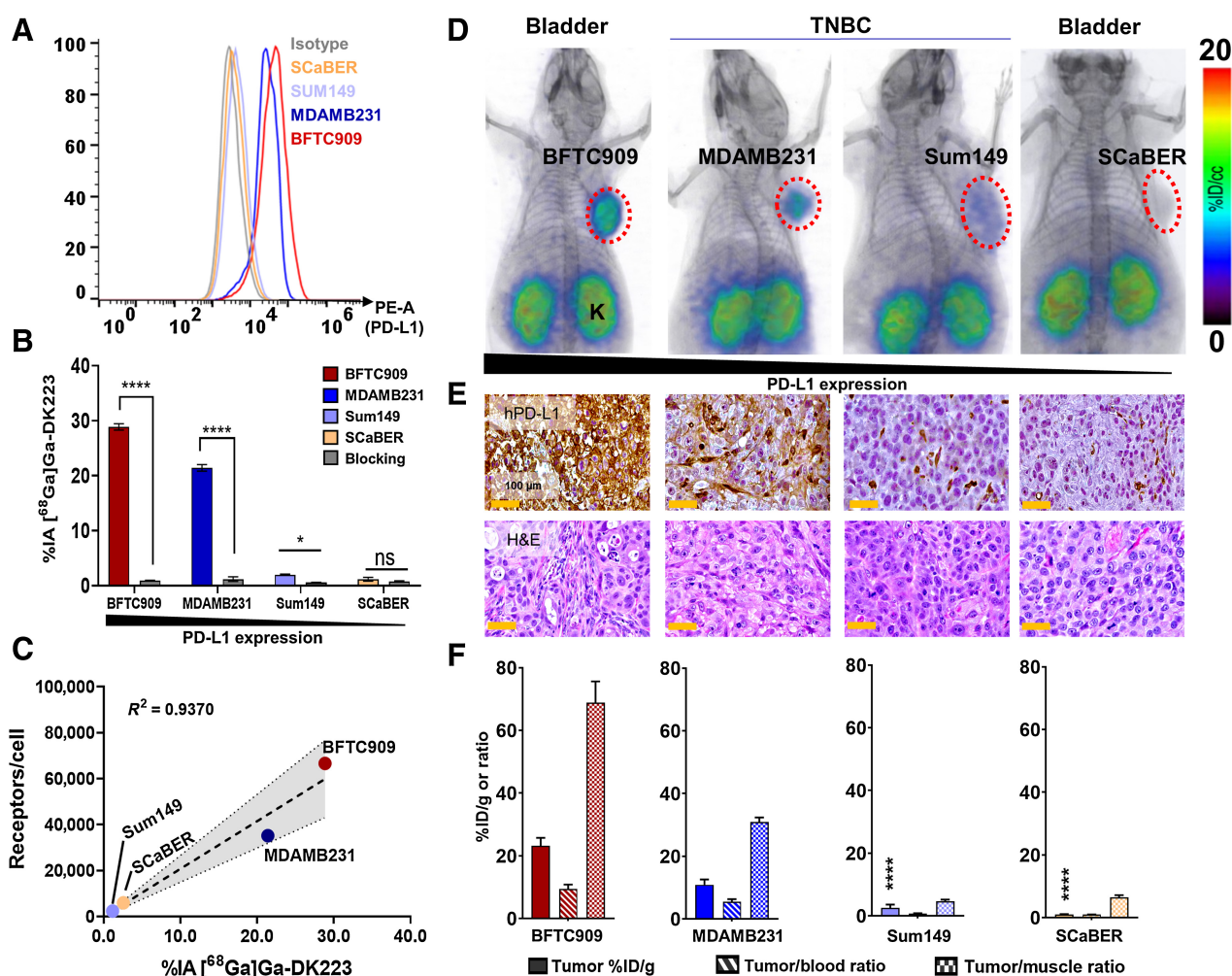
In addition to testing human tumor xenografts of natural expressing PD-L1, we also tested [<sup>68</sup>Ga]Ga-DK223 in genetically

engineered cell lines and tumors with constitutive PD-L1 expression, specifically CHO<sup>hPD-L1</sup>, and corresponding negative controls. Both *in vitro* cell uptake and PET imaging studies showed hPD-L1 uptake in CHO<sup>hPD-L1</sup> and not in CHO cells and tumors (Supplementary Fig. S4A–S4C). Moreover, to evaluate the potential of [<sup>68</sup>Ga]Ga-DK223 to detect inducible PD-L1 expression that is seen during ICT, we employed a genetically engineered cell line A549<sup>iPD-L1</sup> that induces hPD-L1 upon doxycycline treatment.

Induced PD-L1 expression was first validated by flow cytometry using cells that were treated with 1 μg/mL doxycycline for 48 hours (Supplementary Fig. S5A and S5B). PD-L1 expression was significantly higher in A549<sup>iPD-L1</sup> cells treated with doxycycline, and we also observed increased [<sup>68</sup>Ga]Ga-DK223 uptake in a radiotracer binding assay (Supplementary Fig. S5C). Furthermore, we observed high [<sup>68</sup>Ga]Ga-DK223 uptake *in vivo* in A549<sup>iPD-L1</sup> tumors by PET imaging and no increase in uptake in A549 tumors (Supplementary Fig. S5D and S5E). This confirmed the ability of [<sup>68</sup>Ga]Ga-DK223 to detect inducible PD-L1 levels *in vivo*. Taken together, these results demonstrate that [<sup>68</sup>Ga]Ga-DK223 can detect the variability in PD-L1 levels in tumors *in vivo*.

#### PD-L1 mAb exposure in the tumor is quantified by measuring accessible PD-L1 levels using [<sup>68</sup>Ga]Ga-DK223 PET

Three PD-L1 mAbs (atezolizumab, avelumab, and durvalumab) have been approved by the FDA for the treatment of metastatic UC. The overall response rate to these therapeutics is 13% to 25%, with higher response rates observed in patients with high PD-L1 expression (25). The plasmatic exposure–efficacy relationship analysis of these therapeutics did not indicate a significant relationship, suggesting that more robust indicators are needed to guide therapy in UC (21). We reasoned that differences in PD-L1 antibody exposure in the tumors could be estimated by quantifying accessible PD-L1 levels using [<sup>68</sup>Ga]Ga-DK223 PET (Fig. 4A and B). To demonstrate


**Figure 3.**

Evaluation of [<sup>68</sup>Ga]Ga-DK223 in UC and TNBC xenografts. **A**, Flow cytometry analysis of surface expression of PD-L1 in different cancer cell lines. **B**, *In vitro* uptake of [<sup>68</sup>Ga]Ga-DK223 in different cell lines. [<sup>68</sup>Ga]Ga-DK223 uptake is PD-L1 expression dependent, and co-incubation with 1 μmol/L of unlabeled peptide reduced uptake confirming PD-L1 specificity. **C**, *In vitro* [<sup>68</sup>Ga]Ga-DK223 uptake correlates with PD-L1 receptor density. **D**, PET-CT images of NSG mice bearing UC and TNBC tumors at 60 minutes showing PD-L1 specific tumor uptake. Mice were injected with ~ 7.4 MBq (~200 μCi; n = 2-3; B, bladder; K, kidney). **E**, IHC staining for PD-L1 of the corresponding tumors. **F**, Tumor and tumor-to-normal tissue uptake derived using [<sup>68</sup>Ga]Ga-DK223 *ex vivo* biodistribution studies in NSG mice bearing respective cancer xenografts (n = 3-5). Mice were injected with ~ 740 kBq (~20 μCi) and sacrificed after 60 minutes. \*\*\*\*, P < 0.0001 by unpaired Student *t* test when compared with either MDAMB231 or BFTC909 tumors. Simple linear regression and Pearson coefficient were used in **C**.

the feasibility of this approach, we selected two PD-L1 antibodies, avelumab and durvalumab, with distinct biophysical properties. In particular, avelumab has a shorter half-life (6.1 vs. 18 days) and weaker affinity (0.7 vs. 0.02 nmol/L) than durvalumab (20). We first evaluated whether mAb binding to PD-L1 could be assessed using [<sup>68</sup>Ga]Ga-DK223 incubated with BFTC909 cells in the presence (60 nmol/L) or absence of mAb (Fig. 4C). In the absence of mAbs, a 27.9% uptake was observed, but less than 1% uptake was observed in presence of mAbs, indicating that [<sup>68</sup>Ga]Ga-DK223 can only bind accessible PD-L1 not bound by avelumab or durvalumab. No significant difference in [<sup>68</sup>Ga]Ga-DK223 binding was observed between mAb treatments. Extending this observation in *in vivo* experiments, we performed baseline [<sup>68</sup>Ga]Ga-DK223 PET imaging in BFTC909 xenografts, where we observed high radiotracer uptake in the tumors (Fig. 4D). Mice were then treated with 10 mg/kg of avelumab or durvalumab, and [<sup>68</sup>Ga]Ga-DK223 PET images were acquired at 24, 48, 72, and

120 hours after treatment (Fig. 4E; Supplementary Fig. S6). At 24 hours, we observed a significantly lower uptake of [<sup>68</sup>Ga]Ga-DK223 in the tumors of mice treated with mAbs, reflecting the low accessibility of PD-L1 *in vivo*. At 72 hours, avelumab-treated mice showed increased [<sup>68</sup>Ga]Ga-DK223 uptake in tumors compared with durvalumab. At 120 hours, avelumab-treated mice showed [<sup>68</sup>Ga]Ga-DK223 uptake similar to that of saline controls. In contrast, [<sup>68</sup>Ga]Ga-DK223 uptake in durvalumab-treated mice was low due to the low accessibility of PD-L1, indicating that durvalumab remained bound to PD-L1.

To confirm pharmacodynamic effects of avelumab and durvalumab treatments, we performed biodistribution studies. Mice were treated with either avelumab or durvalumab (10 mg/kg) for 24, 48, 72, 96, or 120 hours prior to radiotracer injection, and saline-treated mice were used as controls. Saline-treated mice showed an average of 15%ID/g uptake in tumors, which was significantly reduced by more than 80%

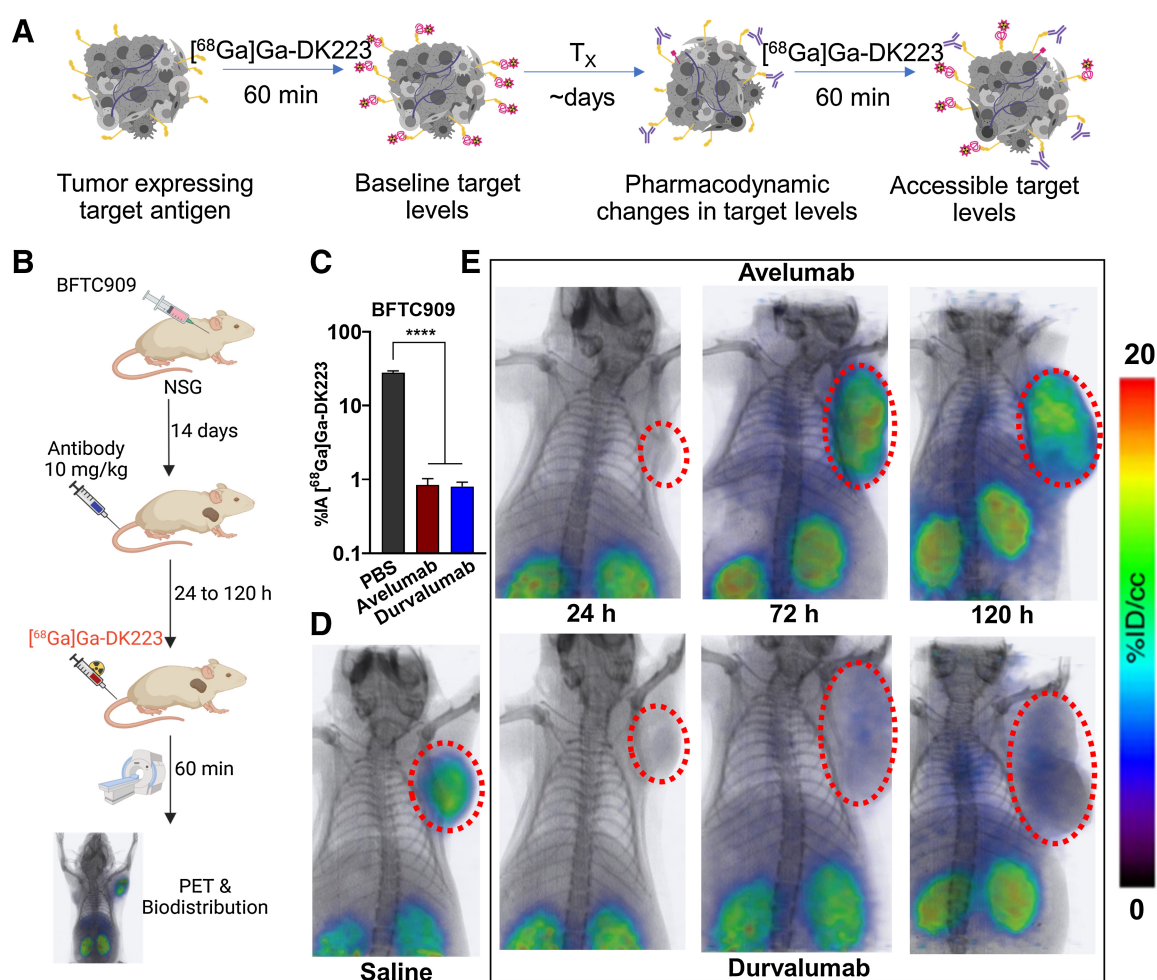


**Figure 4.**

$[^{68}\text{Ga}]\text{Ga-DK223}$  PET reveals temporal differences in tumor exposure of PD-L1 antibodies in BFTC909 xenografts. **A**, Schematic showing measurement of accessible target levels (PD-L1) by  $[^{68}\text{Ga}]\text{Ga-DK223}$  after mAb treatment (created with BioRender.com). **B**, Experimental schematic. **C**,  $[^{68}\text{Ga}]\text{Ga-DK223}$  uptake in BFTC909 cells with and without the presence of 60 nmol/L of aPD-L1 mAbs. Reduced uptake is observed in the presence of mAbs, confirming the ability of  $[^{68}\text{Ga}]\text{Ga-DK223}$  to measure only accessible PD-L1 in presence of mAbs. **D**,  $[^{68}\text{Ga}]\text{Ga-DK223}$  PET-CT image of saline-treated NSG mice bearing BFTC909 tumor at 60 minutes showing high tumor uptake ( $n = 3$ ). **E**, Longitudinal PET-CT study of mice bearing BFTC909 tumors and treated with 10 mg/kg of either avelumab (top) or durvalumab (bottom) for different duration of treatment ( $n = 2-3$ ). All images were acquired 60 minutes after injection of  $\sim 7.4 \text{ MBq}$  ( $\sim 200 \mu\text{Ci}$ )  $[^{68}\text{Ga}]\text{Ga-DK223}$ . \*\*\*\*,  $P < 0.0001$  by unpaired Student *t* test.

( $P < 0.0001$ ) after 24-hour treatment with avelumab (Fig. 5A). However, no significant differences in  $[^{68}\text{Ga}]\text{Ga-DK223}$  uptake were observed between the avelumab-treated mice and saline controls at 120 h. In contrast, durvalumab-treated mice showed a continued reduction in accessible target levels even at 120 hours, corroborating the PET imaging results (Fig. 5B). A similar trend was observed in tumor-to-blood and tumor-to-muscle ratios, with no significant difference in uptake in nonspecific tissues between mAb treatment groups at any time point (Supplementary Fig. S7A and S7B). To measure the fraction of accessible PD-L1 bound by mAbs, we analyzed the tumor %ID/g in the treatment groups as a fraction of the saline treatment group. At 24 hours, both antibodies showed  $\sim 90\%$  reduction in accessible PD-L1 levels, indicating a significant exposure of mAbs (binding of mAbs to PD-L1) within the tumor microenvironment (Fig. 5C). After 120 hours of treatment, we noticed an increase in accessible PD-L1 levels in avelumab-treated mice, in contrast to less than 10% accessible PD-L1 levels in durvalumab-treated mice. These

results demonstrate that measurements of accessible PD-L1 levels could provide insights into mAb exposure kinetics in tumors. In addition, these results show the potential of relating the dose to the exposure of mAb therapeutics in tumors over the course of treatment.

## Discussion

In this study, we established that a novel  $^{68}\text{Ga}$ -labeled radio-tracer,  $[^{68}\text{Ga}]\text{Ga-DK223}$ , binds specifically to PD-L1 with high affinity ( $1.01 \pm 0.83 \text{ nmol/L}$ ) and enables noninvasive quantification of PD-L1 levels as early as 60 minutes post-administration, a process that takes days when using radiolabeled antibodies, such as  $[^{89}\text{Zr}]\text{atezolizumab}$ . Although radiolabeled antibodies provide valuable information about drug distribution and accumulation *in vivo*, they are drug-centric and deriving target engagement information from those measurements is complex. Furthermore, measurements of radiolabeled antibodies by PET comprise a

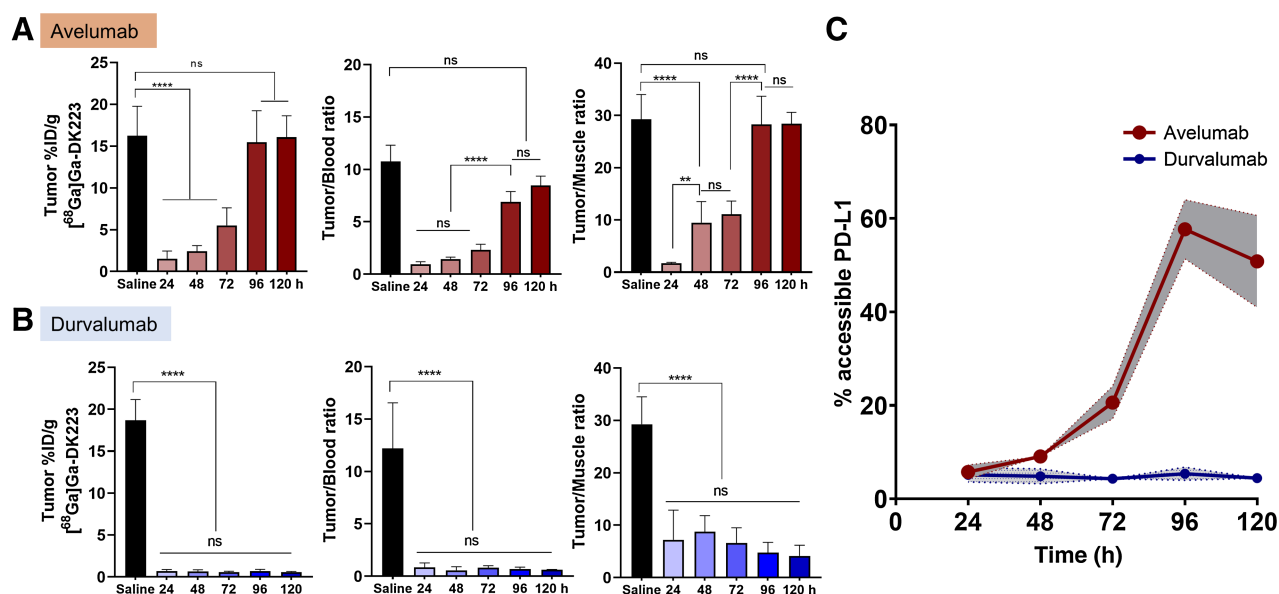


**Figure 5.** Quantification of accessible PD-L1 levels using  $[^{68}\text{Ga}]\text{Ga-DK223}$  in BFTC909 xenografts. *Ex vivo* biodistribution studies in NSG mice bearing BFTC909 tumors treated with 10 mg/kg of either avelumab or durvalumab for 24, 48, 72, 96, or 120 hours. Mice were injected with  $\sim 740$  kBq ( $\sim 20$   $\mu\text{Ci}$ )  $[^{68}\text{Ga}]\text{Ga-DK223}$  and sacrificed 60 minutes after injection. Tumor %ID/g and tumor-to-tissue ratios over different duration of treatment of (A) avelumab, and (B) durvalumab ( $n = 5-6$ ). C, % of accessible PD-L1 levels in tumor calculated as fraction of average untreated control ( $n = 5$ ). Shaded region represents 95% confidence interval. \*\*,  $P < 0.01$ ; \*\*\*,  $P < 0.001$ ; \*\*\*\*,  $P < 0.0001$  by two-way ANOVA.

combination of target expression, antibody accumulation in the tumor, and residualization of the radionuclide, and are thus significantly influenced by factors intrinsic and extrinsic to the tumor.

Also, as antibody distribution is significantly influenced by biophysical properties, such measurements cannot be used to compare the effectiveness of different therapeutics. In contrast,  $[^{68}\text{Ga}]\text{Ga-DK223}$  PET measurements are target-centric, independent of antibody characteristics, and inclusive of factors intrinsic and extrinsic to the tumor.

Our experiments also demonstrated that  $[^{68}\text{Ga}]\text{Ga-DK223}$  can be used to quantify baseline and accessible PD-L1 levels, i.e., levels that are not occupied by mAb therapeutics during treatment. *In vivo* measurements using tumor xenograft models validated the ability of this radiotracer to evaluate the pharmacodynamics of two different PD-L1 therapeutics within tumors. With the growing scope of immunotherapy and more mAbs in development, this approach shows promise for establishing dose-exposure-response relationships, screening patients to predict the benefit from therapy, and monitoring the efficacy of PD-L1 treatment in a more personalized fashion. We envision that  $[^{68}\text{Ga}]\text{Ga-DK223}$  PET clinical application will be similar to  $[^{18}\text{F}]\text{FDG}$  PET, once timing of the on-treatment scan is optimized, for monitoring immune checkpoint therapies.

Dose-exposure-response relationships play an important role in drug development, particularly in dose selection and optimization. The maximum tolerated dose is often used as a strategy for cytotoxic agent development, but it is difficult to apply to immune checkpoint inhibitors, as several agents do not reach MTD (26). Moreover, dose-exposure-response relationships of immune checkpoint therapeutics are often confounded by a complex interplay of patient characteristics, including Eastern Cooperative Oncology Group status, number of metastatic sites, baseline tumor burden, cancer-related cachexia, lac-

tate dehydrogenase level, body weight, and albumin concentration (21). Exposure to these agents is often measured as acute or integrated drug concentrations in plasma and other biological fluids to model and predict occupancy at the tumor (27). However, evaluation of pharmacodynamic markers focused on receptor occupancy indicates that parameters obtained from plasma samples are poor surrogates for the tumor pharmacokinetics of mAbs (28). Our study demonstrates a novel and robust approach to understand the temporal kinetics of aPD-L1 mAbs in tumors using PD-L1 PET to establish dose-exposure relationships.

Patient selection for PD-1 or PD-L1 targeted therapeutics is often based on PD-L1 levels in the index lesion, as tumors with high PD-L1 levels demonstrate a better response (29). mAb conjugates and small protein imaging agents have been used to account for the heterogeneity and dynamics of PD-L1 expression (17, 18). However, there is still a need for imaging agents with tractable pharmacokinetics and high tumor-to-background ratios. Here, we show that the low-molecular-weight peptide  $[^{68}\text{Ga}]\text{Ga-DK223}$  meets these criteria and provides high-contrast images of PD-L1 within 60 minutes of administration in human tumor xenografts derived from TNBC and UC.  $[^{68}\text{Ga}]\text{Ga-DK223}$  detects total and inducible PD-L1 levels in the tumor micro-environment, whether it is a tumor- or immune cell-based expression (30). Data from the phase III KEYNOTE-355 trial in patients with TNBC showed that patients with high PD-L1 expression at baseline [combined positive score (CPS)] responded better to the PD-1 inhibitor pembrolizumab (31). Similarly, CPS-based stratification also guides ICT in UC (32). The increasing use of CPS as a biomarker suggests that  $[^{68}\text{Ga}]\text{Ga-DK223}$  PET measurements could be used to quantify total PD-L1 levels in the whole body to guide therapy (13).

Notably,  $^{68}\text{Ga}$ -based imaging agents are being used increasingly in nuclear medicine, with multiple new agents recently receiving approval (33, 34). Gallium-68 can be obtained using a  $^{68}\text{Ge}/^{68}\text{Ga}$  generator,

enabling kit-based formulations that facilitate radiotracer dissemination. Recently, cyclotron-produced gallium-68 provides even larger quantities of this isotope for radiotracer synthesis.

To enable routine noninvasive pharmacodynamic measurements, a high-affinity radiotracer with *in vivo* target specificity is essential. In addition to meeting these needs, [<sup>68</sup>Ga]Ga-DK223 also inhibits PD-1: PD-L1 interactions with lower affinity than that of antibodies, a property that allows it to bind PD-L1 that is not bound by aPD-L1 mAbs, such as avelumab or durvalumab. Population pharmacokinetic models of these mAbs suggest that they have similar clearance profiles, but different half-lives (35). However, the mechanism by which these biophysical properties affect exposure and target engagement at the tumor remains unknown (36). Here, we have shown that [<sup>68</sup>Ga]Ga-DK223 can be used to measure baseline and accessible PD-L1 levels during treatment with these mAbs. PET imaging revealed that although both mAbs sufficiently bound accessible PD-L1 levels, as measured by [<sup>68</sup>Ga]Ga-DK223 at 24 hours, there were stark differences at later time points. While these differences may appear to reflect the pharmacokinetic profile of the mAbs, several baseline factors, such as patient intrinsic characteristics, demographic factors, and disease-related factors, could influence exposure within the tumor but are difficult to quantify otherwise. For example, cachexia is one of the most important disease-related baseline factors that can confound the exposure–response relationships of immune checkpoint therapeutics (37). Our studies were performed in immunocompromised mice due to specificity of [<sup>68</sup>Ga]Ga-DK223 towards hPD-L1. Development of new mouse and human cross-reactive analogs could provide more mechanistic insights into immunotherapy responses. Taken together, our data suggest that [<sup>68</sup>Ga]Ga-DK223 PET measurements provide a noninvasive, drug-independent approach to quantify the pharmacodynamic effects of such factors on tumor exposure to therapeutics. On the basis of these results, further studies in humans are warranted.

### Authors' Disclosures

D. Kumar reports non-financial support from D&D Pharmatech and Precision Molecular Inc. during the conduct of the study; in addition, D. Kumar has a patent for PCT/US2017/068025 pending to Johns Hopkins University Licensed by D&D Pharmatech/PMI. R.F. Hobbs reports grants from NIH/NCI during the conduct of the study, as well as other support from Radiopharmaceutical Imaging and Dosimetry, LLC outside the submitted work. R.F. Hobbs is Chair of the AAPM (American

Association of Physicists in Medicine) Radiopharmaceutical Therapy Subcommittee. In addition, R. Hobbs has a patent for Application No. 12/687,670 with royalties paid from Rapid, LLC. S.P. Rowe reports grants and personal fees from Precision Molecular, Inc. during the conduct of the study. S. Nimmagadda reports grants, personal fees, and non-financial support from D&D Pharmatech and Precision Molecular Inc., during the conduct of the study; in addition, S. Nimmagadda has a patent (PCT/US2017/068025) pending to Johns Hopkins University. No disclosures were reported by the other authors.

### Authors' Contributions

**A. Mishra:** Conceptualization, data curation, writing—original draft, writing—review and editing. **D. Kumar:** Conceptualization, data curation, writing—original draft, writing—review and editing. **K. Gupta:** Data curation, writing—review and editing. **G. Lofland:** Data curation, writing—review and editing. **A.K. Sharma:** Methodology, writing—review and editing. **D.S. Banka:** Data curation, formal analysis. **R.F. Hobbs:** Formal analysis, writing—review and editing. **R.F. Dannals:** Methodology, writing—review and editing. **S.P. Rowe:** Funding acquisition, methodology, writing—review and editing. **E. Gabrielson:** Data curation, methodology, writing—review and editing. **S. Nimmagadda:** Funding acquisition, methodology, conceptualization, data curation, writing—original draft, writing—review and editing.

### Acknowledgments

This study was funded by NIH R01CA269235 (S. Nimmagadda and S.P. Rowe), NIH 1R01CA236616 (S. Nimmagadda), the Allegheny Health Network-Johns Hopkins Cancer Research Fund (S. Nimmagadda), and NIH P41EB024495. Core resources (histology and imaging) were supported by NIH P30CA006973. We thank Drs. Martin Pomper and Seulki Lee for their support; Precision Molecular, Inc./D&D Pharmatech for providing the Germanium-68/Gallium-68 generator; and Drs. John T. Poirier and Charles Rudin for the gift of A549<sup>hPD-L1</sup> cell line. We thank Dr. Ravindra DeSilva for assistance with installation and initial evaluation of Germanium-68/Gallium-68 generator. We thank Drs. Aykut Üren and Purushottam Tiwari at Georgetown University for performing SPR experiments.

The publication costs of this article were defrayed in part by the payment of publication fees. Therefore, and solely to indicate this fact, this article is hereby marked "advertisement" in accordance with 18 USC section 1734.

### Note

Supplementary data for this article are available at Clinical Cancer Research Online (<http://clincancerres.aacrjournals.org/>).

Received June 21, 2022; revised October 6, 2022; accepted November 22, 2022; published first November 30, 2022.

### References

- Anagnostou V, Landon BV, Medina JE, Forde P, Velculescu VE. Translating the evolving molecular landscape of tumors to biomarkers of response for cancer immunotherapy. *Sci Transl Med* 2022;14:1–14.
- Glassman PM, Balthasar JP. Physiologically based pharmacokinetic modeling to predict the clinical pharmacokinetics of monoclonal antibodies. *J Pharmacokinet Pharmacodyn* 2016;43:427–46.
- Jain RK. Physiological barriers to delivery of monoclonal antibodies and other macromolecules in tumors. *Cancer Res* 1990;50:814s–9s.
- Bartelink IH, Jones EF, Shahidi-Latham SK, Lee PRE, Zheng Y, Vicini P, et al. Tumor drug penetration measurements could be the neglected piece of the personalized cancer treatment puzzle. *Clin Pharmacol Ther* 2019;106:148–63.
- Trédan O, Galmarini CM, Patel K, Tannock IF. Drug resistance and the solid tumor microenvironment. *J Natl Cancer Inst* 2007;99:1441–54.
- Weissleder R, Schwaiger MC, Gambhir SS, Hricak H. Imaging approaches to optimize molecular therapies. *Sci Transl Med* 2016;8:1–8.
- de Vries EGE, Kist de Ruijter L, Lub-de Hooge MN, Dierckx RA, Elias SG, Oosting SF. Integrating molecular nuclear imaging in clinical research to improve anticancer therapy. *Nat Rev Clin Oncol* 2019;16:241–55.
- Gandini S, Massi D, Mandalà M. PD-L1 expression in cancer patients receiving anti PD-1/PD-L1 antibodies: a systematic review and meta-analysis. *Crit Rev Oncol Hematol* 2016;100:88–98.
- Gong J, Chehrizi-Raffle A, Reddi S, Salgia R. Development of PD-1 and PD-L1 inhibitors as a form of cancer immunotherapy: a comprehensive review of registration trials and future considerations. *J Immunother Cancer* 2018;6:1–18.
- Bellmunt J, Powles T, Vogelzang NJ. A review on the evolution of PD-1/PD-L1 immunotherapy for bladder cancer: The future is now. *Cancer Treat Rev* 2017; 54:58–67.
- Chatterjee S, Lesniak WG, Gabrielson M, Lisok A, Wharram B, Sysa-Shah P, et al. A humanized antibody for imaging immune checkpoint ligand PD-L1 expression in tumors. *Oncotarget* 2016;7:10215–27.
- Mansfield AS, Dong H. Implications of programmed cell death 1 ligand 1 heterogeneity in the selection of patients with non-small cell lung cancer to receive immunotherapy. *Clin Pharmacol Ther* 2016;100:220–2.
- Nimmagadda S. Quantifying PD-L1 expression to monitor immune checkpoint therapy: opportunities and challenges. *Cancers* 2020;12:1–26.

14. Doroshov DB, Bhalla S, Beasley MB, Sholl LM, Kerr KM, Gnjatic S, et al. PD-L1 as a biomarker of response to immune checkpoint inhibitors. *Nat Rev Clin Oncol* 2021;18:345–62.
15. Taube JM, Anders RA, Young GD, Xu H, Sharma R, McMiller TL, et al. Colocalization of inflammatory response with B7-h1 expression in human melanocytic lesions supports an adaptive resistance mechanism of immune escape. *Sci Transl Med* 2012;4:127ra37.
16. Bensch F, van der Veen EL, Lub-de Hooge MN, Jorritsma-Smit A, Boellaard R, Kok IC, et al. 89Zr-atezolizumab imaging as a noninvasive approach to assess clinical response to PD-L1 blockade in cancer. *Nat Med* 2018;24:1852–8.
17. Donnelly DJ, Smith RA, Morin P, Lipovšek DA, Gokemeijer J, Cohen D, et al. Synthesis and biologic evaluation of a novel 18 F-labeled adnectin as a PET radioligand for imaging PD-L1 expression. *J Nucl Med* 2018;59:529–35.
18. Lesniak WG, Mease RC, Chatterjee S, Kumar D, Lisok A, Wharram B, et al. Development of [18F]FPy-WL12 as a PD-L1 specific PET imaging peptide. *Mol Imaging* 2019;18:1536012119852189.
19. Zhou X, Jiang J, Yang X, Liu T, Ding J, Nimmagadda S, et al. First-in-human evaluation of a PD-L1-binding peptide radiotracer in non–small cell lung cancer patients with PET. *J Nucl Med* 2022;63:536–42.
20. Kumar D, Lisok A, Dahmane E, McCoy M, Shelake S, Chatterjee S, et al. Peptide-based PET quantifies target engagement of PD-L1 therapeutics. *J Clin Invest* 2019;129:616–30.
21. Centanni M, Moes DJAR, Trocóniz IF, Ciccolini J, van Hasselt JGC. Clinical pharmacokinetics and pharmacodynamics of immune checkpoint inhibitors. *Clin Pharmacokinet* 2019;58:835–57.
22. Chatterjee S, Lesniak WG, Miller MS, Lisok A, Sikorska E, Wharram B, et al. Rapid PD-L1 detection in tumors with PET using a highly specific peptide. *Biochem Biophys Res Commun* 2017;483:258–63.
23. Kumar D, Mishra A, Lisok A, Kureshi R, Shelake S, Plyku D, et al. Pharmacodynamic measures within tumors expose differential activity of PD(L)-1 antibody therapeutics. *Proc Natl Acad Sci USA* 2021;118:e2107982118.
24. Matthew MM, et al. Macrocyclic inhibitors of the PD-1/PD-L1 and CD80(B7-1)/PD-L1 protein/protein interactions. 2014.
25. Lu S, Stein JE, Rimm DL, Wang DW, Bell JM, Johnson DB, et al. Comparison of biomarker modalities for predicting response to PD-1/PD-L1 checkpoint blockade: a systematic review and meta-analysis. *JAMA Oncol* 2019;5:1195–204.
26. Balar AV, Weber JS. PD-1 and PD-L1 antibodies in cancer: current status and future directions. *Cancer Immunol Immunother* 2017;66:551–64.
27. Deng R, Bumbaca D, Pastuskovas CV, Boswell CA, West D, Cowan KJ, et al. Preclinical pharmacokinetics, pharmacodynamics, tissue distribution, and tumor penetration of anti-PD-L1 monoclonal antibody, an immune checkpoint inhibitor. *MAbs* 2016;8:593–603.
28. Brahmer JR, Tykodi SS, Chow LQM, Hwu W-J, Topalian SL, Hwu P, et al. Safety and activity of anti-PD-L1 antibody in patients with advanced cancer. *N Engl J Med* 2012;366:2455–65.
29. Büttner R, Gosney JR, Skov BG, Adam J, Motoi N, Bloom KJ, et al. Programmed death-ligand 1 immunohistochemistry testing: a review of analytical assays and clinical implementation in non–small cell lung cancer. *J Clin Oncol* 2017;35:3867–76.
30. Liu Y, Zugazagoitia J, Ahmed FS, Henick BS, Gettinger SN, Herbst RS, et al. Immune cell PD-L1 colocalizes with macrophages and is associated with outcome in PD-1 pathway blockade therapy. *Clin Cancer Res* 2020;26:970–7.
31. Heeke AL, Tan AR. Checkpoint inhibitor therapy for metastatic triple-negative breast cancer. *Cancer Metastasis Rev* 2021;40:537–47.
32. Powles T, Eder JP, Fine GD, Braithel FS, Loriot Y, Cruz C, et al. MPDL3280A (anti-PD-L1) treatment leads to clinical activity in metastatic bladder cancer. *Nature* 2014;515:558–62.
33. Banerjee SR, Pomper MG. Clinical applications of Gallium-68. *Appl Radiat Isot* 2013;76:2–13.
34. Willmann JK, van Bruggen N, Dinkelborg LM, Gambhir SS. Molecular imaging in drug development. *Nat Rev Drug Discov* 2008;7:591–607.
35. Sheng J, Srivastava S, Sanghavi K, Lu Z, Schmidt BJ, Bello A, et al. Clinical pharmacology considerations for the development of immune checkpoint inhibitors. *J Clin Pharmacol* 2017;57:S26–42.
36. Simon GM, Niphakis MJ, Cravatt BF. Determining target engagement in living systems. *Nat Chem Biol* 2013;9:200–5.
37. Roch B, Coffy A, Jean-Baptiste S, Palaysi E, Daures J-P, Pujol J-L, et al. Cachexia-sarcopenia as a determinant of disease control rate and survival in non–small lung cancer patients receiving immune-checkpoint inhibitors. *Lung Cancer* 2020;143:19–26.